

Observation of Carrier Distribution in Compound Semiconductors Using Off-axis Electron Holography

by Hirokazu Sasaki *, Shinya Ootomo *, Takeyoshi Matsuda * and Hirotatsu Ishii *

ABSTRACT

It is well known that carrier distribution in semiconductors can be observed by using electron holography, and many such studies on Si semiconductors have been reported. In this paper, sample preparation and observation techniques are optimized with the aim of improving the observation technology of carrier distribution in compound semiconductors. The authors have been successful in making clear observation of the p-n junction in GaAs semiconductor, as well as in clearly distinguishing between the n^+ layer and n^- layer. The techniques developed here are applicable to various semiconductor products such as lasers, holding promise for contributing to performance and reliability improvements.

1. INTRODUCTION

In the development of various semiconductor devices, it is essential to confirm whether the structure is fabricated as designed or not, as well as to identify their electrical performance. Typical means of structural observation are SEM (Scanning Electron Microscopy) for low-power observation and TEM (Transmission Electron Microscopy) for high-power observation, and these means play an important role not only in research and development but also in product management. Ordinary TEM methods --capable of obtaining transmission images, bright-field images, dark-field images, and high-resolution images, etc.-- allow for real space observation of such information as crystal orientation, distribution of dislocations, and crystallinity, making themselves an indispensable evaluation technique in the development of semiconductor materials. However, it is impossible for these TEM methods to obtain magnetic and/or electric field information on minute parts. Information on these micro structures is needed in the development of devices using semiconductors and magnetic materials in some cases, and electron holography is one of the techniques that meet this requirement.

Electron holography is the application of holography techniques invented by Gabor¹⁾ to electron waves. Historically, Tonomura et al. implemented the in-line electron holography²⁾, and the off-axis electron holography was realized using the biprism invented by Möllenstedt³⁾. Since then, with the improvement in measuring equipment, numbers of remarkable fruits of research in magnetic field observation have been reported⁴⁾, including magnetic field distribution in magnetic materials and superconductive single flux quantum.

Frabboni et al. succeeded in the observation of semi-

conductors using electron holography for the first time in 1985⁵⁾. In their experiment, the electric field around the p-n junction of Si caused by application of an electric voltage was observed. The experimentation is pioneering in the sense that this is the first application of electron holography to semiconductors. McCartney et al. was successful in the direct observation of the p-n junction in semiconductors, which was reported in 1994⁶⁾. In 1999, Rau et al. first applied the technique to a practical device. They were successful in the observation of Si MOSFET, report of which triggered the observation of semiconductors based on electron holography by many research institutes. Then Wang et al. succeeded in observing Si MOSFET prepared as a TEM sample using FIB (Focused Ion Beam)⁸⁾, and Twitchett et al. reported on their study on amplified electrostatic potential at a p-n junction generated by the application of an electric voltage⁹⁾.

All the observation examples thus far were made on Si semiconductors, and no observations ever were made on the p-n junction of compound semiconductors. Since Furukawa Electric's semiconductor products belong to the compound semiconductor groups, we embarked on the study of electron holography observation techniques for compound semiconductors such as GaAs and InP. In this paper, the outline and techniques for electron holography observation of compound semiconductors are presented, along with quantitative discussions on the experimental results.

2. OTHER TECHNIQUES FOR CARRIER DISTRIBUTION OBSERVATION

Other evaluation techniques for dopant distribution and carrier distribution in semiconductors include those by SIMS (Secondary Ion Mass Spectrometry), SEM¹⁰⁾, and SCM (Scanning Capacitance Microscopy)¹¹⁾. In this

* Yokohama Research Lab., R&D Div.

Section, these techniques are described for their characteristics, and are compared with electron holography.

SIMS is a surface analysis technique in which a primary ion beam is irradiated on the sample surface, and the secondary ions emitted through sputtering phenomenon are measured to evaluate the chemical composition of the surface. SIMS is capable of evaluating trace amounts of dopants, and its sensitivity is extremely high. Its high sensitivity, while depending on the combination of the sample matrix and dopant, can evaluate low-concentration dopants in the range of $1.0 \times 10^{13} \sim 1.0 \times 10^{16} \text{ cm}^{-3}$, making it indispensable equipment for material and device development. Being a depth profile analysis technique, however, it is basically used for one-dimensional analysis.

SEM is an analysis technique in which a focused electron beam is used to irradiate the object, and secondary electrons and backscattered electrons emitted from the object are detected. In case SEM is used for semiconductor surface observation, it is possible to observe the p-n contrast using a cleaved surface. Being an easy-to-use evaluation technique, it is very useful in the manufacturing and development fields. In terms of SEM contrast, information resulting from surface irregularities and different compositions are often utilized, but in the case of semiconductors, it is known that contrast is also generated by the kind and quantity of dopants¹⁰. Since the SEM technique is significantly influenced by oxygen and the like adsorbed on semiconductor surfaces, it is somewhat difficult to make quantitative evaluation. However, it is now extensively used for its ease of observation using simple-to-prepare cleaved samples.

SCM is a kind of scanning probe microscope in which a probe is used to scan the surface of a semiconductor sample, whereby it detects the p-n contrast by measuring the electric capacitance on the surface. Since SCM gathers information with a depth of several tens nanometers from the surface rather than several nanometers, it enables quantitative evaluation without being influenced by the conditions of extremely shallow surfaces. The spatial resolution of SCM is, while depending on the quality of the metal probe tip, around several tens nanometers.

Electron holography is the method for measuring the inner potential of a sample. In comparison to the various methods mentioned above, this method has its own advantages and disadvantages, but its most remarkable advantage is that it has high spatial resolution. Therefore, as the semiconductor devices decrease in size, it is becoming an indispensable technique in the development sectors for Si devices. Since it is a technique for evaluating electrostatic potential distribution, it may be defined as an indirect evaluation technique for carrier distribution.

3. PRINCIPLE OF SEMICONDUCTOR OBSERVATION USING ELECTRON HOLOGRAPHY

3.1 Electron Holography Technique

Electron holography, a kind of TEM techniques, became widely known for its successful validation of the Aharonov-

Bohm effect¹²⁾. Historically this technique has been broadly used in the fundamental physics, achieving very remarkable results. But it has been less widely used in the laboratories of private companies for observation of practical materials.

Figure 1 illustrates how two electron waves emitted from an electron source with coherence reaches an observer after passing through two trajectories. In order to understand the physical phenomenon of electron waves observed by this observer, the Schrödinger equation shown below has to be solved.

$$\left[\frac{1}{2m} \{-i\hbar \cdot \nabla + eA(r)\}^2 - V(r) \right] \psi(r) = E\psi(r) \quad (1)$$

where e , m , and ψ are the charge, rest mass, and wave function of electron, respectively; and \hbar is Dirac's constant, E is the energy of electron, A is the vector potential, and V is the scalar potential. In electron holography, the equation can be solved by using a phase integral technique of the WKB method to obtain the phase change which is expressed as follows:

$$\Delta\phi = \oint_C \left(k + \frac{V}{2E} k - \frac{eA}{\hbar} \right) ds \quad (2)$$

where k is the wavenumber. The first term on the right-hand side represents the phase change due to the optical path difference. This term can be ignored in the experimental system of electron holography, since the electron trajectories 1 and 2 have the same optical path. The second term represents the phase change due to electrostatic potential. The third term represents the contribution of vector potential A , reflecting the conditions of the magnet-

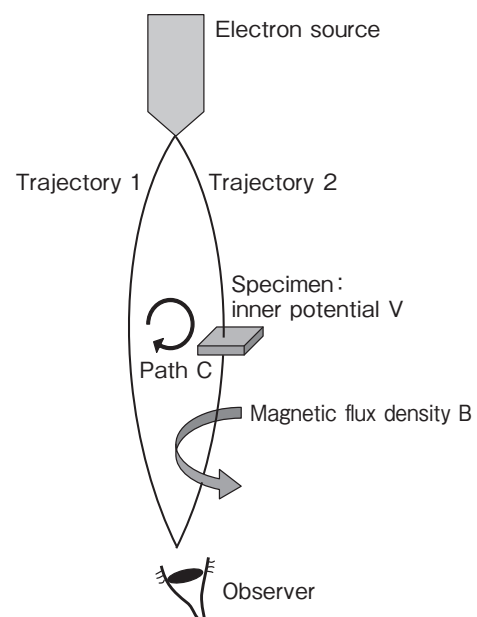


Figure 1 Phase measurement of electron wave.

ic flux. Thus as shown in Figure 1, both the inner potential change in a sample placed in the electron trajectory and the flux that penetrates the area enclosed by the electron trajectory can be observed as the phase change of a wave function. The observation of carrier distribution in semiconductors described in this paper takes advantage of the information on the inner potential represented in this second term.

3.2 Relationship between Electrostatic Potential and Phase Difference

It is widely known that electrostatic potential distribution in semiconductors such as the p-n junction can be observed by using electron holography. This is because differing electrostatic potentials can be expressed as a phase difference of electron waves as shown in the following equation:

$$\Delta\phi = \frac{\pi}{\lambda E} Vt \quad (3)$$

where λ is the wavelength of electron wave and E is the energy of electron beam, and hence $\pi/\lambda E$ is a constant. Furthermore, t is the sample thickness, V is the potential. From Equation (3), the electrostatic potential distribution can be observed, if the thickness of TEM sample is uniform, by detecting the phase distribution.

At the p-n junction, an electrostatic potential distribution is formed such that the Fermi levels come into coincidence. Thus while the n-type and p-type semiconductors from the same kind of semiconductor have almost the same mean inner potential, the resulting mean inner potential has the same distribution as for the electrostatic potential, due to the Fermi level shift. More specifically, using electron holography, it becomes possible to measure this inner potential that underwent an apparent change.

4. OBSERVATION OF COMPOUND SEMICONDUCTORS BY ELECTRON HOLOGRAPHY: IN CASE OF SAMPLES PREPARED BY CLEAVING

4.1 Advantages of Cleaved Samples

As can be seen from Equation (3) where the thickness information as t is included in the right-hand side, the information on sample thickness appears in the phase image if the TEM sample has thickness nonuniformity. It is necessary, therefore, to prepare a TEM sample with a uniform thickness. However, since this requirement for sample thickness uniformity is higher in electron holography than in standard TEM, it is difficult to fabricate a sample with amply uniform thickness by means of TEM sample preparation techniques relying on mechanical polishing and Ar ion milling alone. Even when the FIB technique is used for sample preparation, the damaged layer on the TEM sample surface formed during the FIB process may

have a great influence raising a substantial problem. The damaged layer consists of fine crystals and amorphous substances, with a thickness up to 30 nm in some cases, and causes noise in the phase information. For these reasons, the TEM samples for the measurement presented here were prepared by cleaving. The cleaved TEM sample permits quantitative discussions, because, in spite of the fact that its thickness changes, the rate of change remains constant.

4.2 Observation of p-n Junction in Compound Semiconductors Using Cleaved Samples

4.2.1 Observation Conditions

As the electron holography observation equipment, we used a Hitachi HF-2000 equipped with an FE (Field Emission) electron gun. The electron beam acceleration voltage was 200 kV. The phase image was reconstructed using Fourier transformation.

4.2.2 Observation Samples

The p-n junctions of GaAs were observed. The p-type GaAs was doped with silicon with a dopant concentration of $1.0 \times 10^{18} \text{ cm}^{-3}$; while the n-type GaAs was doped with carbon with a dopant concentration of $2.0 \times 10^{18} \text{ cm}^{-3}$. The samples were prepared by cleaving. Figure 2 shows the procedure of sample preparation. As shown, two cleaved surfaces were exposed by two cleaving operations, and subsequently the cleaved sample was mounted with a tilt angle of 45° on to the TEM holder.

4.2.3 Observation Results

Figure 3 shows the hologram and phase image obtained. The downside of the image corresponds to the vacuum region. In the phase image shown in Figure 3 (b), the position of the p-n junction is clearly visible. Also it can be seen that the phase jump has larger deflections in the thicker layers.

4.2.4 Analysis of Phase Image

An attempt was made to quantitatively obtain, from the phase image shown in Figure 3 (b), the potential difference between the p-type and n-type semiconductors. The phase change due to the inner potential and the sample thickness can be expressed, as has been described above, by the following equation:

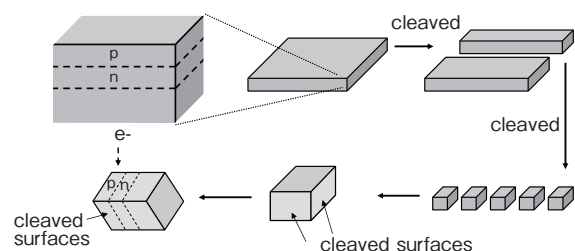


Figure 2 Preparation of cleaved samples for electron holography.

$$\Delta\phi = \frac{\pi}{\lambda E} Vt \equiv C_E Vt \quad (4)$$

where C_E has replaced the constant term.

In this experiment, the edge has a 90° angle since the sample is cleaved, and when the sample is tilted to 45° from the horizontal, the following relation is determined:

$$t = 2x \quad (5)$$

where x is the distance from the sample edge, t is the sample thickness. Hence the following relationship is derived from Equations (4) and (5).

$$V = \frac{1}{C_E} \frac{d\phi}{dt} = \frac{1}{2C_E} \frac{d\phi}{dx} \equiv \frac{1}{2C_E} \alpha \quad (6)$$

where $d\phi/dx$ is replaced by α . From the above, the following equation is established:

$$V_n - V_p = \frac{1}{2C_E} (\alpha_n - \alpha_p) \quad (7)$$

To perform numerical analysis, as shown in Figure 4, an averaged phase profile over the p-type and n-type regions is created from the phase image, and α_n and α_p are obtained from the slope of the profile. Here, $V_n - V_p$ was calculated from the slope $\alpha_n - \alpha_p$, and the result was 1.2 eV.

On the other hand, the difference between the Fermi levels of p-GaAs(2×10^{18}) and n-GaAs(1×10^{18}) was calculated to be approximately 1.35 eV, showing moderate agreement between the measured and calculated values. The disagreement may be attributable to the influence of surface depletion layer to be described later and the inaccuracy in the inclination angle, and so on¹²⁾.

5. OBSERVATION OF COMPOUND SEMICONDUCTORS BY ELECTRON HOLOGRAPHY: IN CASE OF SAMPLES PREPARED BY FIB

5.1 Necessity of Removing FIB Damaged Layer

Preparation of TEM samples becomes very important in the application of electron holography to compound semiconductors. Use of FIB, although its capability of processing any specific part on the device is advantageous, may pose the problem of forming a damaged layer on the sample. This problem is particularly significant with semiconductors such as GaAs, GaN, and InP, such that use of a Ga ion beam with an acceleration voltage of 30~40 kV can form a damaged layer of several tens nm in thickness on the processed surface. It is the characteristic of these damaged layers that, unlike those in Si, fine crystals coexist in an amorphous substance layer¹³⁾. These fine crystals is very problematic in that, when making electron holographic observations, the electron waves transmitting through these fine crystals are influenced by diffraction contrast, resulting in noise generation. In their observation experiments on the GaAs p-n junctions using electron holography, Cooper et al. were unable to reconstruct clear phase images from TEM samples prepared by FIB alone¹⁴⁾. They resorted to crystal recovery by annealing the TEM sample in situ, thereby succeeding in obtaining a clear image. Although this in situ annealing is one of the possible solutions, it is not necessarily applicable to any materials, and in addition, a more rapid sample preparation technique is desirable from the standpoint of observing actual devices.

Accordingly, we have applied in this work another technique to the preparation of TEM samples for electron holographic observations, in which as shown in Figure 5, the damaged layer is removed by Ar ion milling after FIB processing. This technique enables reducing the FIB damaged layer down to several nanometers in thickness¹³⁾.

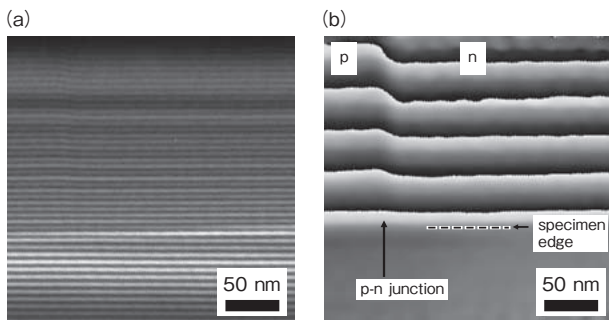


Figure 3 (a)Hologram and (b) phase image of p-n junction in GaAs cleaved sample.

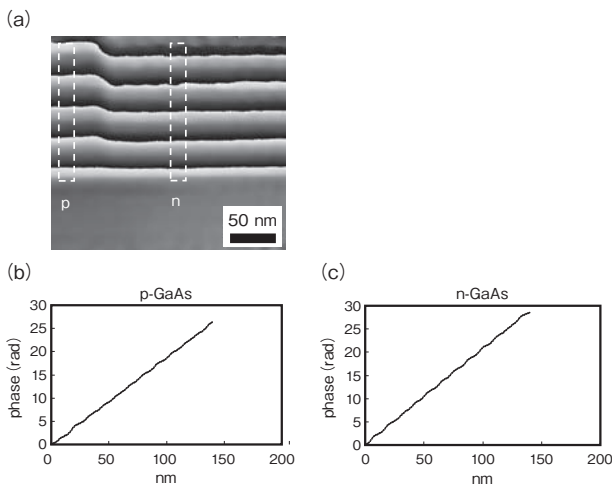


Figure 4 Hologram and phase profiles of p-type region and n-type region.

5.2 Observation of Compound Semiconductor Samples by Electron Holography

5.2.1 Observation Samples

Figure 6 shows a schematic diagram of the sample used for observation. It is a model sample in which thin layers of p-GaAs and n-GaAs are deposited on a GaAs substrate using MOCVD. In the n-GaAs layer, a high-concentration n^+ region and a low-concentration n^- region have been fabricated. The dopants for this sample are silicon for the n-GaAs and carbon for the p-GaAs. The dopant concentrations determined by SIMS for the n^- layer, n^+ layer, and p layer are $1.3 \times 10^{16} \text{ cm}^{-3}$, $3.0 \times 10^{18} \text{ cm}^{-3}$, and $1.0 \times 10^{19} \text{ cm}^{-3}$, respectively.

5.2.2 TEM Sample Preparation Conditions

FIB was used for sample preparation. The FIB processing equipment is a Hitachi FB-2100. A Ga ion beam of 40 kV in acceleration voltage was used. The TEM sample was processed to a thickness of 300 nm while monitoring the thickness by SIM (Scanning Ion Microscope) image observation. After the FIB processing, Ar milling was performed at room temperature. The Ar milling equipment is a GATAN dual ion milling; the incident angle of the Ar ion beam is 10° ; and the sample was Ar ion milled for five minutes without being rotated.

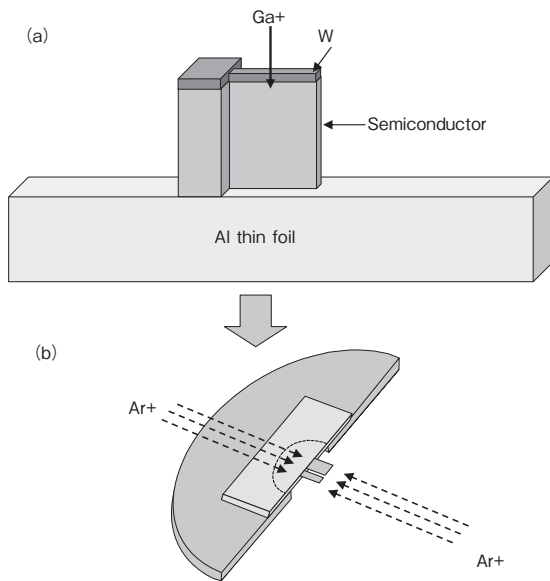


Figure 5 Preparation of TEM samples using FIB and Ar milling.

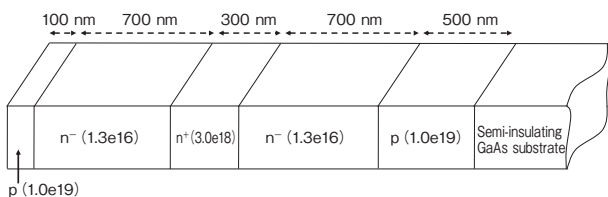


Figure 6 Schematic diagram of the GaAs p-n-p test sample.

5.2.3 Measurement Conditions for Phase Shifting Electron Holography

Observations were made using a JEOL-3000F equipped with an FE electron gun. The acceleration voltage for the electron gun was 300 kV. The holograms were imaged using a GATAN 794 CCD camera with 1024×1024 pixels. Under the observation conditions adopted, one pixel of CCD camera corresponds to 2 nm in size. The voltage applied on the biprism was 13 V. The phase shifting method¹⁵⁾ was employed for reconstructing the phase images, and 13 holograms were taken.

5.2.4 Observation Results

Figure 7 shows a transmission electron micrograph. A tungsten protection layer against FIB processing is located on the left-side of the sample. As has been revealed by this transmission electron micrograph, it is impossible to observe contrast between the regions with different dopants. Figure 8 (a) shows one of the holograms and Figure

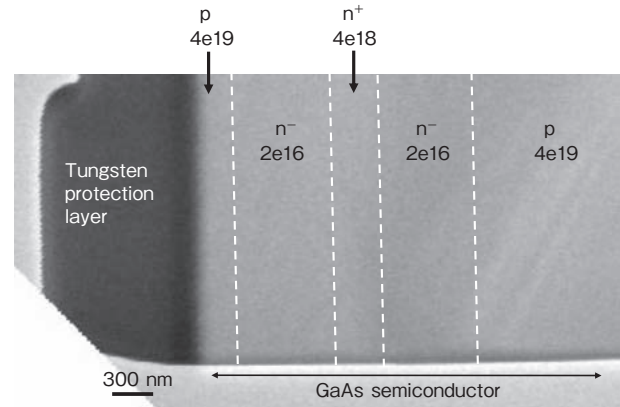


Figure 7 Transmission electron micrograph of FIB-prepared GaAs sample with p, n^+ , and n^- regions.

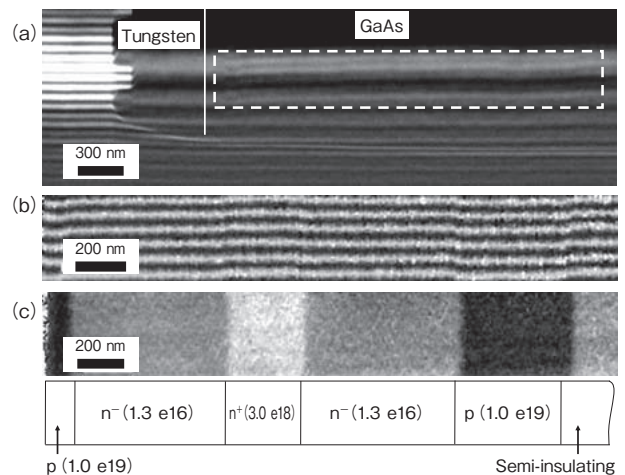


Figure 8 (a) Electron hologram obtained from GaAs sample. (b) Corrected hologram without Fresnel fringes obtained from the region enclosed by broken lines shown in (a). (c) Reconstructed phase image obtained from 13 holograms.

8 (b) shows interference fringes obtained from the region enclosed by broken lines shown in Figure 8 (a), after the Fresnel fringes are removed and contrast adjusted. It can be confirmed that, whereas in Figure 8 (a) the interference fringes are invisible under the influence of Fresnel fringes, they become clearly visible by the removal of Fresnel fringes, showing deflections at the interface between the regions with different dopants. It may be noted that the spacing between the interference fringes is about 60 nm. Figure 8 (c) shows a phase image reconstructed from 13 holograms. This phase image shows that the p region is clearly distinguishable from the n region and that the n^- region and n^+ region can be clearly distinguished as well¹⁶⁾.

5.2.5 Discussions

Figure 9 shows the averaged phase profile generated for the purpose of interpreting the phase image shown in Figure 8 (c). The phase difference across the p and n^- regions is about 1.1 rad, and the one across the n^+ and n^- regions is about 0.8 rad. Figure 10 shows the electrostatic potential profile generated using the dopant concentration obtained from SIMS measurements. The profile was

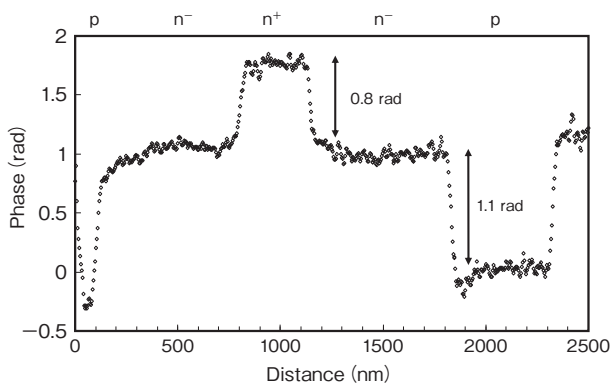


Figure 9 Averaged phase profile across p-n junction and n^+/n^- interface obtained from phase image.

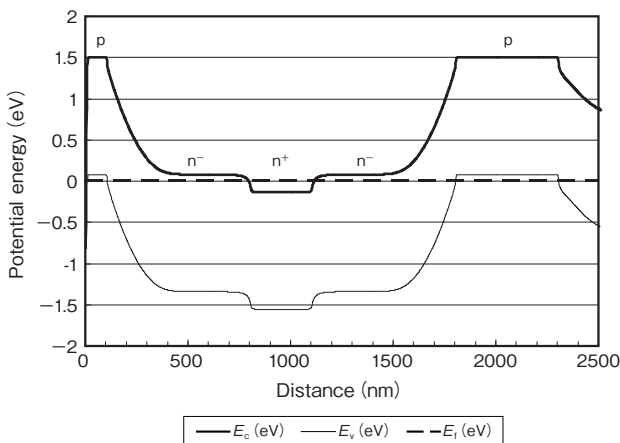


Figure 10 Band diagram of sample obtained by solving Poisson's equations self-consistently.

generated by Band Calculator. In this profile, the electrostatic potential across the n^- and p regions is about 1.4 eV, and the one across the n^+ and n^- regions is about 0.2 eV. The relationship between the electrostatic potential difference and the phase difference can be expressed by the following equation, which is a modification of Equation (4) that takes into account the effects of the layer damaged at the time of sample preparation:

$$\phi = C_E V (t - 2t_0) \quad (8)$$

where t_0 is the thickness of a damaged layer. It should be noted that Equation (8) is valid when the electrostatic potential stays constant along the direction of the electron beam in the TEM sample. Whereas Equation (8) indicates that the electrostatic potential difference and the phase difference are in a linear relationship, the results of this experiment shows that the phase difference and the electrostatic potential difference for the n^- and p regions are 1.1 rad and 1.4 eV, respectively, and that the phase difference and the electrostatic potential difference for the n^+ and n^- regions are 0.8 rad and 0.2 eV, respectively, thus contradicting a linear relationship. This contradiction may be attributed to invalidity of Equation (8), or more specifically, to the fact that the electrostatic potential fluctuates along the transmission direction of the electron beam. In such a case, the following equation should be used to express the relationship between the electrostatic potential and phase:

$$\phi = C_E \int_0^{t-2t_0} V(z) dz \quad (9)$$

where z is the component along the transmission direction of the electron wave. To determine the changes in the electrostatic potential and carrier distribution along the z direction, a simulation was carried out taking into consideration the potential changes in the z direction. Figure 11 shows the directions along which the simulation was run. The simulation was carried out under several assumptions such that the Fermi levels on the sample surface from the bottom end of conductor are 0.90 eV for p-GaAs and 0.65 eV for n-GaAs, respectively^{17), 18)}, and that all the dopants are activated. The TEM sample thickness was determined by CBED (Convergent Beam Electron Diffraction) measurement to be 280 nm.

Figure 12 shows the simulation results for the band dia-

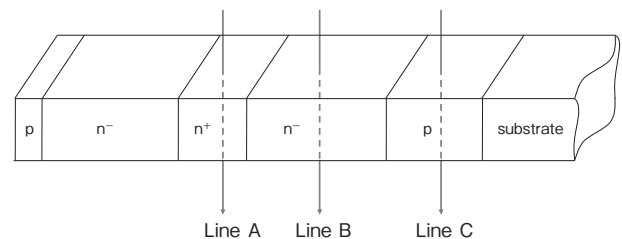


Figure 11 Schematic diagram of the directions along which simulations were run.

gram and the carrier concentration, in which Figure 12 (a) and (b) show those for the n^+ region, Figure (c) and (d) for the n^- region, and Figure (e) and (f) for the p region. It can be seen that, in the n^+ and p regions of high dopant concentration, the bands are bent sharply near the surface of a TEM sample. Also, it can be confirmed from the carrier concentration profiles that the carriers are decreased near the surface, forming a depletion layer. On the other hand, the n^- region is under significantly different conditions from those of bulk substances. That is to say, the carriers disappear as can be seen in Figure 12 (d), and the bands are globally bent as shown in the band diagram in Figure 12 (c). The Fermi level is located approximately at the middle of the bandgap, thus indicating remarkably different characteristics compared to intrinsic n semiconductors. From the above, the experimental results suggest that whereas the depletion layer exists only near the TEM sample surface for the p and n^+ regions, it extends to the entire TEM sample for the n^-

region.

Based on these results and using Equation (9), we recalculated the phase difference. The result shows that the phase differences across the n^- and p regions ($\Delta \phi_{n-p}$) and the n^+ and n^- regions ($\Delta \phi_{n+n^-}$) are 1.62 rad and 1.11 rad, respectively. These results are in better agreement with the experimental results than before in terms of linear relationship, but the agreement is still insufficient. This is attributable to the influence of an electric inactive layer that has been formed by the Ga ion beam. Assuming that a 40-nm thick electric inactive layer exists on the TEM sample surface, we have a new set of $\Delta \phi_{n-p}$ and $\Delta \phi_{n+n^-}$ values of 1.08 rad and 0.84 rad, respectively, resulting in good agreement with the experimental results.

Figure 13 shows a cross-sectional structure of TEM sample that is deduced from the experimental results above described. A damaged layer due to FIB, consisting of amorphous substances and fine crystals existed on the surface but this was removed by Ar milling, so that a dam-

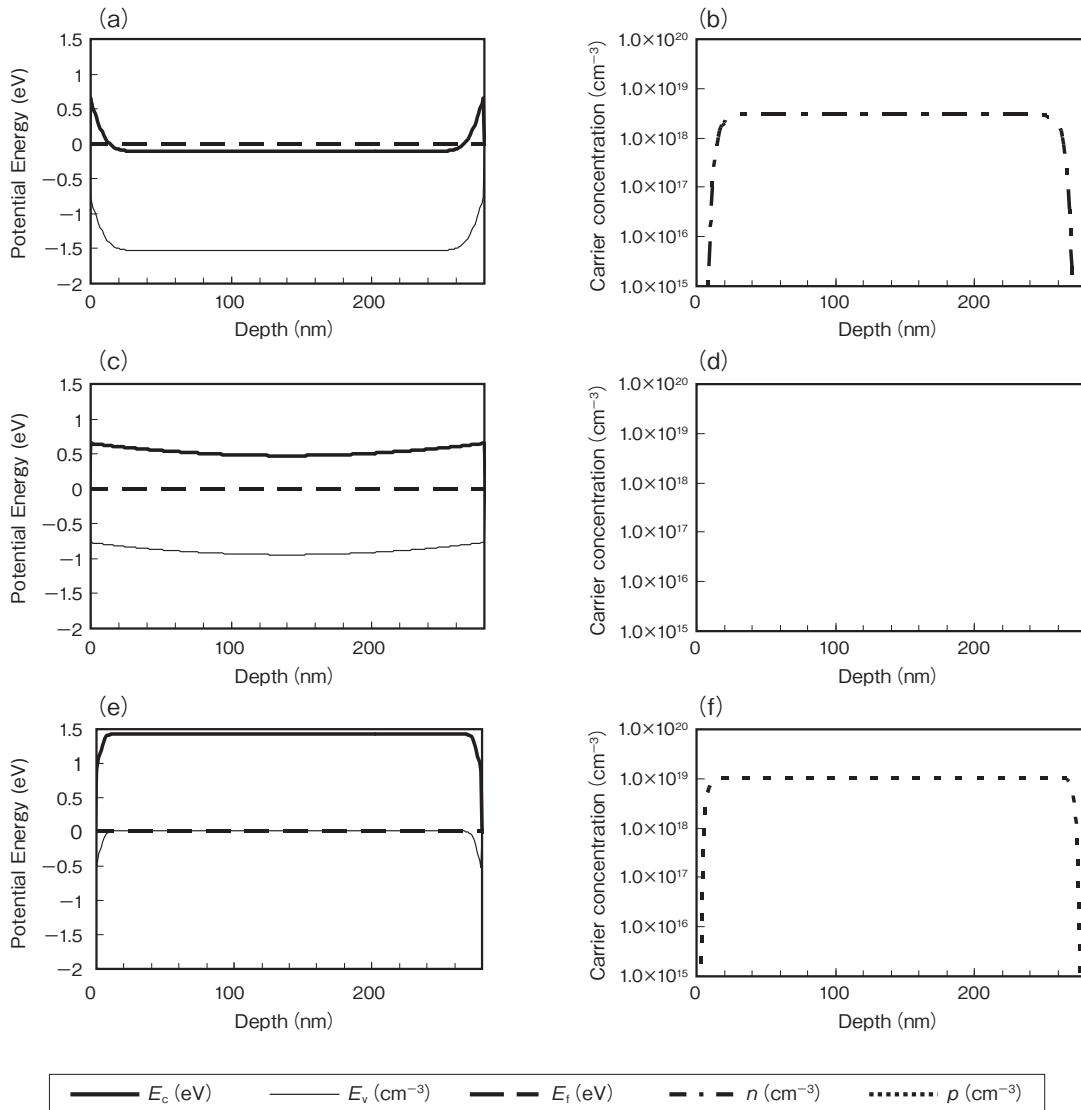


Figure 12 Simulations of the band diagram and carrier concentration in the TEM sample. (a) band diagram and (b) carrier concentration for the n^+ region along line A. (c), (d) those for the n^- region along line B. (e), (f) those for p region along line C.

aged layer several nanometers in thickness due to Ar milling is thought to be present. Under the damaged layer, an electric inactive layer formed by Ga ion milling or Ar milling exists; under which a depletion layer is present with a thickness that depends on the dopant concentration. With respect to the sample observed here, the entire n^- region of the sample is supposed to be depleted.

6. CONCLUSION

The electrostatic distributions in GaAs have been successfully observed using electron holography. This means indirect observation of carrier distributions, since electrostatic distribution corresponds to carrier distribution in the case of semiconductors. It is shown that the use of a cleaved sample allow clear observation of p-n junction. The technique is advantageous in that, although it provides only one-dimensional information, it makes preparation of samples and interpretation of measurement results easy without the need for consideration on FIB damaged layer. In the case of sample preparation using FIB, on the other hand, it is advantageous to remove the FIB damaged layer by means of Ar ion milling, as long as observation is concerned. In our experiments for this case, the results suggest that an electric inactive layer is present on both sides of the TEM sample. In the observation of GaAs, it was possible to distinguish the dopant concentration regions of $1.3 \times 10^{16} \text{ cm}^{-3}$ and $3.0 \times 10^{18} \text{ cm}^{-3}$ in n-type semiconductor, as well as p-n junction. These techniques are applicable to observation of actual devices, making themselves a useful means for improving the performance and reliability of semiconductor devices.

ACKNOWLEDGMENTS

We thank our joint researchers at the Nanostructures Research Laboratory, the Japan Fine Ceramics Center, including Dr. T. Hirayama, Dr. K. Yamamoto, and Dr. Z. Wang (currently with Micron Technology).

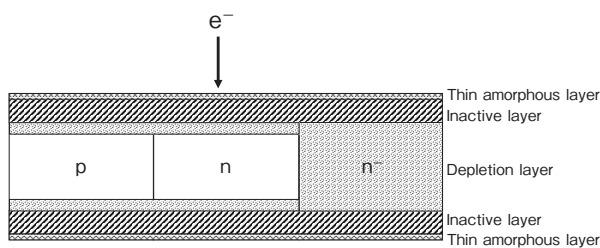


Figure 13 Cross-sectional TEM sample structure deduced by our study.

REFERENCES

- 1) D. Gabor: "A new microscopic principle," *Nature*, 161 (1948), 777.
- 2) A. Tonomura, A. Fukuhara, H. Watanabe and T. Komoda: "Optical reconstruction of image from Fraunhofer electron hologram," *Jpn. J. Appl. Phys.*, 7 (1968), 295.
- 3) G. Mollenstedt and H. Duker: "Fresnel'scher interferenzversuch mit einem biprisma für Elektronenwellen," *Naturwissenschaften*, 42 (1955), 41.
- 4) T. Matsuda, S. Hasegawa, M. Igarashi, T. Kobayashi, M. Naito, H. Kajiyama, J. Endo, N. Osakabe, and A. Tonomura: "Magnetic field observation of a single flux quantum by electron-holographic interferometry," *Phys. Rev. Lett.*, 62 (1989), 2519.
- 5) S. Frabboni, G. Matteucci and G. Pozzi: "Electron holographic observations of the electrostatic field associated with thin reverse-biased p-n junctions," *Phys. Rev. Lett.*, 55 (1985), 2196.
- 6) M. R. McCartney, D. J. Smith, R. Hull, J. C. Bean, E. Voelkl and B. Frost: "Direct observation of potential distribution across Si/Si p-n junctions using off-axis electron holography," *Appl. Phys. Lett.*, 65 (1994), 2603.
- 7) W. D. Rau, P. Schwander, F. H. Baumann, W. Hoppner, and A. Ourmazd: "Two-Dimensional Mapping of the Electrostatic Potential in Transistors by Electron Holography," *Phys. Rev. Lett.*, 82 (1999), 2614.
- 8) Z. Wang, T. Hirayama, K. Sasaki, H. Saka and N. Kato: "Electron holographic characterization of electrostatic potential distributions in a transistor sample fabricated by focused ion beam," *Appl. Phys. Lett.* 80, 246 (2002).
- 9) A. C. Twitchett, R. E. Dunin-Borkowski, and P. A. Midgley: "Quantitative Electron Holography of Biased Semiconductor Devices," *Phys. Rev. Lett.*, 88 (2002), 238302.
- 10) F. Iwase, Y. Nakamura, and S. Furuya: "Secondary electron emission from Si-implanted GaAs," *Appl. Phys. Lett.*, 64 (1994), 1404.
- 11) A. Erickson, L. Sadwick, G. Neubauer, J. Kopanski, D. Adderton and M. Rogers: "Quantitative scanning capacitance microscopy analysis of two-dimensional dopant concentrations at nanoscale dimensions," *J. Electronic Materials*, 25 (1996), 301.
- 12) J. Li, M. R. McCartney, R. E. Dunin-Borkowski and D. Smith: "Determination of mean inner potential of germanium using off-axis electron holography," *Acta Cryst.*, A55 (1999), 652.
- 13) K. Yabusaki, H. Sasaki: "Specimen Preparation Technique for a Microstructure Analysis Using the Focused Ion Beam Process" *Furukawa Review*, 22 (2002).
- 14) D. Cooper, A. C. Twitchett, P. K. Somodi, P. A. Midgley, R. E. Dunin-Borkowski, I. Farrer, and D. A. Ritchie: "Improvement in electron holographic phase images of focused-ion-beam-milled GaAs and Si p-n junctions by in situ annealing," *Appl. Phys. Lett.*, 88 (2006), 063510.
- 15) K. Yamamoto, I. Kawajiri, T. Tanji, M. Hibino, and T. Hirayama, "High precision phase-shifting electron holography," *J. Electron Microsc.* 49 (2000) 31.
- 16) H. Sasaki, K. Yamamoto, T. Hirayama, S. Ootomo, T. Matsuda, F. Iwase, R. Nakasaki, and T. Ishii: "Mapping of dopant concentration in a GaAs semiconductor by off axis phase-shifting electron holography," *Appl. Phys. Lett.*, 89 (2006), 244101.
- 17) W.E. Spicer, P.W. Chye, P.R. Skeath, C.Y. Su and I. Lindau: "New and unified model for schottky barrier and III-V insulator interface states formation," *J. Vac. Sci. Technol.*, 16 (1979), 1422.
- 18) W. Monch: "Chemisorption-induced defects at interfaces on compound semiconductors," *Surf. Sci.*, 132 (1983), 92.